TOPICAL REVIEW — Heat conduction and its related interdisciplinary areas

Optimization strategies for thermal transport properties of n-type Mg_3Sb_2-based thermoelectric alloys

Jiawei Zha(查佳伟)[1], Di Zhang(张娣)[1], and Zhiyuan Liu(刘志愿)[1,2,†]

[1] *School of Materials Science and Engineering, Advanced Ceramics Research Center, Anhui University of Technology, Maanshan* 243002, *China*
[2] *State Key Laboratory of Advanced Technology for Materials Synthesis and Processing, Wuhan University of Technology, Wuhan* 430070, *China*

(Received 12 April 2026; revised manuscript received 18 May 2026; accepted manuscript online 22 May 2026)

The n-type Mg_3Sb_2-based alloys have attracted considerable attention as promising thermoelectric materials for intermediate-temperature applications, owing to their unique layered crystal structure, suitable bandgap, and intrinsically low thermal conductivity. However, the conversion efficiency of thermoelectric devices fabricated from Mg_3Sb_2-based materials remains relatively low, and further enhancement of the thermoelectric figure of merit zT is essential. Since lattice thermal conductivity is weakly coupled to electrical transport parameters, reducing lattice thermal conductivity has become a key strategy for improving the zT of Mg_3Sb_2-based materials. On the one hand, introducing defects and mass-strain field fluctuations via doping or alloying can significantly enhance phonon scattering and reduce lattice thermal conductivity. Simultaneously, this approach can improve electrical transport properties by tuning the carrier concentration. On the other hand, nano-modification and nanocomposite engineering enable control of grain size and microstructure, enhancing carrier and phonon scattering to reduce thermal conductivity without severely degrading electrical performance. This review summarizes recent progress in optimizing the thermal transport properties of n-type Mg_3Sb_2-based alloys through doping/alloying, nano-modification, nanocomposite formation, and synergistic regulation. These strategies enable a substantial reduction in thermal conductivity while maintaining stable electrical properties, leading to significantly enhanced thermoelectric performance, thus providing scientific and technological support for the application of Mg_3Sb_2-based thermoelectric devices.

Keywords: Mg_3Sb_2-based thermoelectric materials, thermal conductivity, lattice thermal conductivity, thermoelectric performance

PACS: 73.50.Lw, 84.60.Rb, 74.25.F–, 74.25.fc

DOI: 10.1088/1674-1056/ae71b0 **CSTR:** 32038.14.CPB.ae71b0

1. Introduction

With the increasing global emphasis on renewable and clean energy, research on thermoelectric materials has gradually become a hot topic in materials science, energy technology, environmental engineering, and related fields. Thermoelectric materials are functional materials that enable direct interconversion between heat and electrical energy, operating on the principles of the Seebeck effect and Peltier effect, showing broad application prospects in thermoelectric cooling and power generation.[1–5] The conversion efficiency of thermoelectric materials is typically evaluated by the dimensionless figure of merit $zT = S^2\sigma T/\kappa$. The Seebeck coefficient S is defined under open-circuit conditions as $S = \Delta V/\Delta T$, where $\Delta T = T_{\rm hot} - T_{\rm cold}$ and $\Delta V = V_{\rm cold} - V_{\rm hot}$; hence, S directly represents the voltage difference (ΔV) generated per unit temperature difference (ΔT). The electrical conductivity σ is determined by $\sigma = ne\mu_{\rm H}$, where n is the carrier concentration, e is the elementary charge, and $\mu_{\rm H}$ is the Hall carrier mobility, T is the absolute temperature, and κ is the thermal conductivity. The thermal conductivity κ consists of two parts: the carrier thermal conductivity $\kappa_{\rm e}$ and the lattice thermal conductivity $\kappa_{\rm L}$. An ideal thermoelectric material should possess high electrical conductivity, a high Seebeck coefficient, and low thermal conductivity. However, the strong coupling among S, σ, and κ arising from scattering mechanisms and band structure makes it challenging to tune these parameters independently. Therefore, synergistically regulating these parameters to enhance zT is a central focus of fundamental research on thermoelectric materials.[6,7]

In recent years, numerous thermoelectric material systems have been systematically investigated, including skutterudites,[8,9] complex alloys,[10] metal chalcogenides,[11] conducting polymers[12] and oxides.[13] Based on their operating temperature range, thermoelectric materials can be classified into near-room-temperature materials (e.g., Bi_2Te_3[14,15] and Ag_2Se[16]), mid-temperature materials, and high-temperature materials (e.g., oxides and half-Heusler compounds). Among mid-temperature thermoelectric materials, systems such as $CoSb_3$,[8] PbTe,[17] SnSe,[18,19] SnTe[20,21] and GeTe[22] exhibit excellent thermoelectric performance. However, the presence of expensive metals (e.g., Te, Co, Ge) or toxic elements (e.g., Pb, Se) limits their practical applications. In contrast, Mg_3Sb_2 is not only a complex Zintl-phase compound with a crystal structure combining

†Corresponding author. E-mail: zhiyuanliu826@ahut.edu.cn

© 2026 Chinese Physical Society and IOP Publishing Ltd. All rights, including for text and data mining, AI training, and similar technologies, are reserved.

CPB Online In Press

ionic and covalent bonding, which facilitates a significant reduction in lattice thermal conductivity κ_L in the $[Mg_2Sb_2]^{2-}$ anionic layers, but also offers the advantages of low cost and high efficiency. Zintl-phase compounds are crystalline materials composed of electropositive metals and electronegative metalloids or nonmetals. They feature complex bonding networks arising from cationic and anionic frameworks and display "phonon-glass, electron-crystal" (PGEC) behavior. Consequently, Mg_3Sb_2 has drawn considerable attention and stands out in the thermoelectric materials community. Mg_3Sb_2-based thermoelectric materials are typical Zintl-phase thermoelectric compounds with an anti-α-La_2O_3 rhombohedral structure (space group: $P\bar{3}m1$).[23] As shown in Fig. 1, the structure consists of alternating anionic $[Mg_2Sb_2]^{2-}$ slabs and cationic Mg^{2+} layers stacked periodically along the c-axis (Fig. 1(a)). Such charge transfer between sublattices is common in Zintl-phase materials and gives rise to various unusual crystal structures and functions.[24] The $[Mg_2Sb_2]^{2-}$ layer forms a two-dimensional network of edge-sharing Sb tetrahedra, each containing a Mg atom, extending along the c-axis (Fig. 1(b)). The Mg ions in the cationic layers are arranged in a triangular pattern with relatively large interatomic distances. Along the c-direction (Fig. 1(c)), a tunnel-like porous structure within the tetrahedral network can be observed. The unique crystal structure of Mg_3Sb_2-based thermoelectric materials imparts both high carrier mobility and low thermal conductivity.

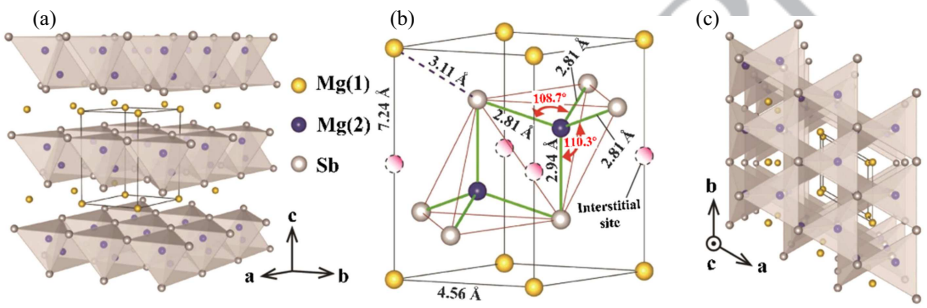


Fig. 1. (a) Perspective view of the Mg_3Sb_2 crystal structure. A unit cell is drawn with black lines. (b) Atom coordination with two Sb tetrahedral (red lines). Interstitial sites (0, 0, 1/2) are also shown. (c) The crystal structure along the c direction.[23]

The high thermoelectric performance of n-type Mg_3Sb_2-based materials is primarily attributed to the ease of achieving a high carrier concentration (e.g., through Sb vacancies or Te doping to provide electrons), as well as the small effective mass and low scattering strength at the conduction band minimum, resulting in a carrier mobility much higher than that of p-type materials. Meanwhile, the conduction band of n-type Mg_3Sb_2 possesses a higher band degeneracy, which allows a large Seebeck coefficient to be maintained while ensuring high electrical conductivity, thereby leading to an excellent power factor; in contrast, p-type Mg_3Sb_2-based materials suffer from low hole concentration caused by intrinsic Mg vacancies, low degeneracy at the valence band maximum, and severe ionized impurity scattering, resulting in poor thermoelectric performance and slow research progress. After decades of development, the zT values of n-type Mg_3Sb_2-based thermoelectric alloys have been significantly enhanced. In particular, important progress has been made in reducing the lattice thermal conductivity, which is weakly correlated with electrical transport parameters. This review mainly summarizes the recent research progress in optimizing the thermal transport properties of n-type Mg_3Sb_2-based materials through doping/alloying, nano-modification, and nanocomposite engineering (Fig. 2). These optimization strategies decouple the thermoelectric parameters and synergistically regulate the electrical and thermal transport properties, leading to a substantial improvement in the zT values of Mg_3Sb_2-based materials. This provides new research directions for developing high-performance thermoelectric materials as well as scientific and technological support for the application of thermoelectric devices.

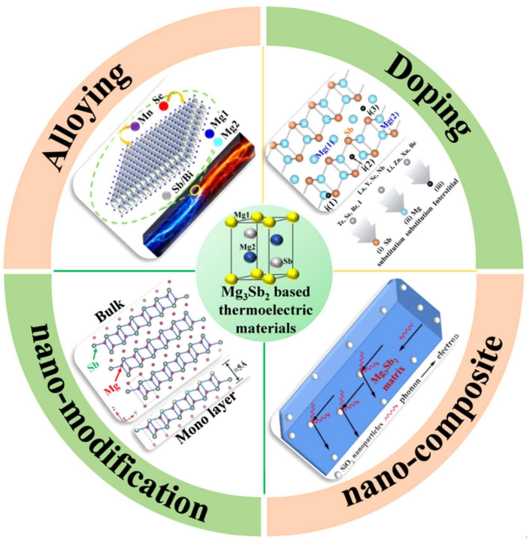


Fig. 2. Optimization strategies for thermal transport properties of n-type Mg_3Sb_2-based thermoelectric materials.[25–28]

2. Strategies for regulating thermal transport performance

Thermal conductivity consists of two components: the carrier thermal conductivity (κ_e) and the lattice thermal con-

ductivity (κ_L) (Eq. (1)). The thermal conductivity in thermoelectric materials originates from two aspects: (i) electrons and holes that transport heat (κ_e); and (ii) phonons traveling through the lattice (κ_L). κ_e is directly related to the electrical conductivity through the Wiedemann–Franz law (Eq. (2)), where L is the Lorenz number (2.4×10^{-8} W·Ω·K^{-2} for heavily degenerate semiconductors), and T is absolute temperature. Consequently, the lattice thermal conductivity κ_L is typically estimated by subtracting κ_e from the measured total κ, $\kappa_L = \kappa - L\sigma T$.

$$\kappa = \kappa_e + \kappa_L, \tag{1}$$

$$\kappa_e = L\sigma T = ne\mu LT. \tag{2}$$

To understand the optimization strategies for thermal transport performance, it is essential to examine the microscopic phonon scattering mechanisms that govern κ_L. Within the framework of the Debye–Callaway model,[7] κ_L can be expressed as an integral over phonon frequency ω:

$$\kappa_L = \frac{k_B}{2\pi^2 v}\left(\frac{k_B T}{\hbar}\right)^3 \int_0^{\theta_D/T} \tau_c(x)\frac{x^4 e^x}{(e^x-1)^2}\,dx, \tag{3}$$

where $x = \hbar\omega/k_B T$, v is the sound velocity, θ_D is the Debye temperature, and τ_c is the total phonon relaxation time. The total scattering rate τ_c^{-1} is determined by various scattering processes via Matthiessen's rule

$$\tau_c^{-1} = \tau_U^{-1} + \tau_D^{-1} + \tau_B^{-1} + \tau_P^{-1} + \cdots. \tag{4}$$

The terms represent Umklapp (U) scattering ($\tau_U^{-1} \propto \omega^2 T\, e^{-\theta_D/bT}$, where b is a dimensionless constant related to the Grüneisen parameter), point defect (D) scattering ($\tau_D^{-1} \propto \omega^4$), boundary (B) scattering ($\tau_B^{-1} = v/d$, where d is grain size), and precipitates (P) scattering, respectively. The strategies discussed below precisely target these individual scattering terms: alloying and doping introduce point defects to enhance high-frequency phonon scattering via the ω^4 Rayleigh term; grain boundary engineering reduces the boundary scattering mean free path d; and nanocomposites create interfaces and precipitates that strongly scatter mid- to low-frequency phonons. Through this multiscale approach, broad-spectrum phonon scattering can be achieved, maximizing the reduction of lattice thermal conductivity. Therefore, optimizing the thermal conductivity of Mg_3Sb_2-based thermoelectric materials primarily involves reducing the lattice thermal conductivity, since the carrier thermal conductivity is inherently coupled with electrical conductivity and is difficult to regulate independently. Currently, three main strategies are employed to reduce the lattice thermal conductivity: (i) introducing point defects (e.g., interstitials, vacancies) through doping or alloying[29–31] to scatter phonons within the unit cell; (ii) tuning the grain size of Mg_3Sb_2-based thermoelectric materials (nano-modification) and implementing defect engineering to enhance phonon scattering, thereby reducing thermal conductivity and improving thermoelectric performance; (iii) introducing a nano-sized second phase into Mg_3Sb_2-based thermoelectric materials to fabricate nanocomposites, utilizing the nano-effects and interfacial effects of the second phase to enhance phonon scattering and significantly reduce the lattice thermal conductivity.

2.1. Defect engineering

Defect engineering, which deliberately introduces point defects, dislocations, and grain boundaries into the Mg_3Sb_2 lattice, has emerged as a primary strategy for decoupling electrical and thermal transport. Alloying and doping, as the most common approaches for creating point defects, will be discussed in detail below.

2.1.1. Alloying and doping strategies

Alloying is a conventional approach to enhance the thermoelectric figure of merit zT of materials.[32] Alloying refers to uniformly mixing two or more metal elements (including small amounts of non-metallic elements) in the molten state or combining them through diffusion in the solid solution state to form new materials with metallic characteristics. Alloying usually significantly alters the structure of the matrix material, with the most common products being solid solutions, intermetallic compounds, and multiphase mixtures. Generally, compared with metals, semiconductors have lower electrical conductivity and a relatively high ratio of thermal conductivity to electrical conductivity, resulting in poor overall performance.[33] However, alloying a material with an appropriate dopant can reduce this ratio, thereby improving the overall performance. In addition, alloying can introduce atomic-scale defects that impede phonon transport and significantly reduce the lattice thermal conductivity. Owing to its narrow bandgap, Mg_3Sb_2 is susceptible to bipolar conduction at elevated temperatures, which severely degrades its thermoelectric performance.[34] Alloying engineering provides an effective route to improve the thermoelectric performance of Mg_3Sb_2-based materials.[28,35–37] Zhang *et al.*[35] selected $SmMg_2Sb_2$-based material, for alloying with $SmMg_2Bi_2$, as it shares the same crystal structure as Mg_3Sb_2. Because Bi atoms are heavier than Sb atoms, the the phonon frequency of $SmMg_2Bi_2$ is significantly lower than that of $SmMg_2Sb_2$. Therefore, alloying with Bi softens the phonons and effectively reduces the lattice thermal conductivity. With the addition of Bi, the lattice thermal conductivity of $SmMg_{2+\delta}Sb_{1.72}Bi_{0.25}Te_{0.03}$ reaches only 0.8 W·m^{-1}·K^{-1} at 873 K, which is 43% lower than that of Bi-free sample ($SmMg_{2+\delta}Sb_{1.97}Te_{0.03}$). Doping Sb into $Mg_{3.2}Bi_{1.99}Se_{0.01}$ leads to solid solution formation between Sb and Bi.[37] Meanwhile, effective phonon scattering caused by

CPB Online In-Press

Bi/Sb disorder reduces the lattice thermal conductivity. Ultimately, high thermoelectric performance is achieved through the synergistic effect of alloying and a tunable bandgap, with disordered Bi/Sb acting as effective phonon scattering centers. The zT value of the $Mg_{3.2}Bi_{1.09}Sb_{0.9}Se_{0.01}$ sample increases from 0.73 at room temperature to 1.28 at 525 K. This demonstrates that alloying is an effective way to improve the thermoelectric performance of n-type Mg_3Sb_2-based materials.

The n-type Mg_3Sb_2-based thermoelectric materials intrinsically possess low lattice thermal conductivity due to strong anharmonicity and low sound velocity. On this basis, introducing foreign dopant atoms to create point defects can further optimize the material's thermal conductivity. Point defects are "zero-dimensional defects" characterized by atomic arrangements that deviate from a perfect lattice. Typically, point defects include vacancies, interstitials, and substitutional atoms. In addition, complex defects occurring over several lattice positions, such as vacancy clusters, interstitial clusters, and cross substitutions, can also be regarded as point defects.[38–40] Figure 3 shows schematic illustrations of various types of point defects, including common simple point defects and complex point defects. Point defects induce lattice distortion and cause the periodic potential to deviate from its equilibrium state, thereby acting as scattering centers for electrons or phonons. Furthermore, point defects can also lead to charge imbalance, resulting in changes in electrical transport properties.

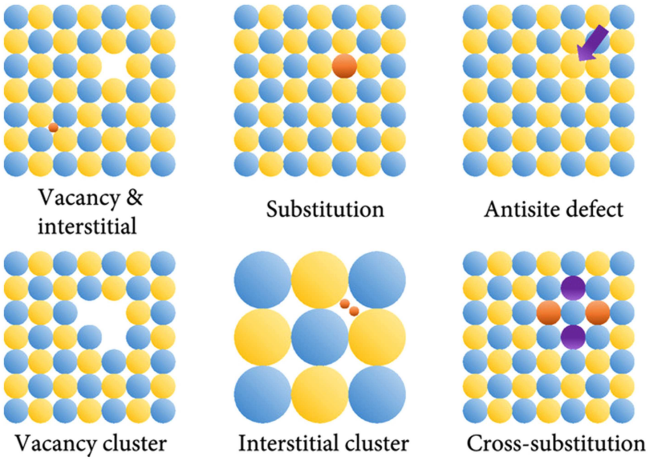


Fig. 3. Schematic diagram of different types of point defects.[41]

Table 1. Thermal transport parameters and zT values of some typical n-type Mg_3Sb_2-based thermoelectric materials prepared by doping different elements.

Sample	κ ($W{\cdot}m^{-1}{\cdot}K^{-1}$)	κ_L ($W{\cdot}m^{-1}{\cdot}K^{-1}$)	zT_{max}	Ref.
$Mg_{3.2}Sb_{1.5}Bi_{0.49}Te_{0.01}$	0.80 @716 K	0.42 @716 K	1.52	[23]
$Mg_{3.18}Mn_{0.02}Sb_{1.5}Bi_{0.49}Se_{0.01}$	0.90 @723 K	0.64 @723 K	1.60	[26]
$Mg_{3.07}Sb_{1.5}Bi_{0.48}Se_{0.02}$	0.618 @725 K	0.46 @725 K	1.23	[43]
$Mg_{3.2}Bi_{1.4}Sb_{0.59}Se_{0.01}$	1.00 @450 K	0.60 @450 K	1.24	[44]
$Mg_{3.17}B_{0.03}Sb_{1.5}Bi_{0.49}Te_{0.01}$	0.70 @1093 K	0.42 @1093 K	1.81	[47]
$Mg_{3.05-x}Y_xSbBi$	1.00 @550 K	0.40 @550 K	1.80	[48]
$Mg_{3.1}Co_{0.1}Sb_{1.5}Bi_{0.49}Te_{0.01}$	0.77 @773 K	–	1.70	[49]
$Mg_{3.2}Y_{0.04}La_{0.01}Sb_{1.5}Bi_{0.5}$	0.75 @750 K	0.39 @750 K	1.76	[50]
$Mg_{3.5}Tm_{0.03}Sb_{1.97}Te_{0.03}$	0.53 @775 K	–	1.75	[51]
$Mg_{3.08-x}Sb_{1.3}Bi_{0.7}Gd_x$	0.80 @700 K	0.50 @700 K	1.55	[52]
$Mg_{3.5}Gd_{0.04}Sb_{1.97}Te_{0.03}$	0.59 @725 K	–	1.26	[53]
$Mg_{3.15}Mn_{0.05}Sb_{1.5}Bi_{0.49}Te_{0.01}$	0.8 @723 K	0.48 @723 K	1.85	[54]
$Y_{0.01}Mg_{3.19}Sb_{1.5}Bi_{0.47}Te_{0.03}$	0.83 @703 K	0.50 @703 K	1.70	[55]

In recent years, the incorporation of various dopants, such as chalcogen elements (Te, Se, etc.),[42–45] group III elements (Y, B, etc.),[46–48] transition metal elements,[49] lanthanide elements (La, Gd, etc.),[50–52] as well as excess Mg, has enabled synergistic optimization of the electrical and thermal transport properties of Mg_3Sb_2-based materials by introducing point defects and tuning the carrier concentration. Mao *et al.*[49] induced atomic mass fluctuations by introducing a large number of point defects through dual doping with Te and the transition metal Co. The dominant ionized impurity scattering changed to a mixture of acoustic phonon and ionized impurity scattering, leading to a significant reduction in lattice thermal conductivity. The $Mg_{3.1}Co_{0.1}Sb_{1.5}Bi_{0.49}Te_{0.01}$ sample achieved a minimum thermal conductivity of 0.79 $W{\cdot}m^{-1}{\cdot}K^{-1}$ at 773 K. Furthermore, in Mg_3Sb_2-based materials, additional cationic doping is also a strategy to improve thermoelectric performance. Yu *et al.*[50] demonstrated that co-doping with rare-earth elements Y and La can simultaneously enhance the power factor and suppress the thermal conductivity of n-type $Mg_{3.2}Sb_{1.5}Bi_{0.5}$. Owing to the additional defect scattering introduced by Y and La, the lattice thermal conductivity was significantly reduced to 0.39 $W{\cdot}m^{-1}{\cdot}K^{-1}$ at 750 K. In the temperature range of 300–750 K, the $Mg_{3.2}Y_{0.04}La_{0.01}Sb_{1.5}Bi_{0.5}$ material achieved a peak zT of 1.76 and an average zT of 1.1. In practice, factors such as solid solubility limits restrict the enhancement of thermoelectric performance achievable through single-element doping. Related experiments have shown that multi-element doping can further improve the thermoelectric performance of n-type Mg_3Sb_2-based materials. Table 1 lists the thermal transport parameters and zT values of some typical Mg_3Sb_2-based thermoelectric materials prepared by doping with various elements in recent years.[23,26,43,44,47–55]

CPB Online

2.1.2. Other defect engineering approaches

Defect engineering is a key thermoelectric technique that precisely controls internal defects (point defects, line defects, planar defects, etc.) to optimize electrical conductivity, Seebeck coefficient, and thermal conductivity, thereby enhancing the zT value. It mainly includes point defects, line defects, and planar defects. Point defects (such as vacancies, substitutional dopants, and interstitials) are the most common, and doping or alloying is an important means of introducing point defects (as discussed in detail above). For example, partially substituting Bi for Sb in Mg_3Sb_2 (substitutional doping) or introducing lattice vacancies can both increase σ by tuning the carrier concentration and scatter phonons to reduce κ. Line defects and planar defects, such as dislocations, grain boundaries, and phase boundaries, are formed by grain refinement or constructing heterostructures. Their main function is to enhance phonon scattering, thereby reducing the lattice thermal conductivity κ_L without significantly affecting electrical transport. In Mg_3Sb_2-based thermoelectric materials, defect engineering primarily aims to tune carrier mobility or concentration (synergistically optimizing σ and S) while disrupting phonon propagation paths (reducing κ), thus breaking the bottleneck of "electrical–thermal coupling". Li *et al.*[56] proposed a method to reduce carrier scattering by Mg vacancies, thereby enhancing mobility. Simultaneously, increasing the sintering temperature promotes Bi volatilization, generating more Bi-related defects and significantly enhancing phonon scattering. Furthermore, to maintain charge balance, the contents of Mg and Bi were reduced. As a result, with increasing Bi vacancies (V_{Bi}) and the Sb/Bi ratio, a lower κ_L was achieved under off-stoichiometric conditions, indicating that more vacancies introduced additional defects. Combined with a high power factor (PF) and low κ_L, the $Mg_{3.19}Y_{0.01}Sb_{1.5}Bi_{0.5}$ sample attained a peak zT of 1.82 at 773 K.

2.2. Nano-modification

"Nano-modification" refers to a design strategy that optimizes the thermoelectric performance of materials by introducing nanoscale structures or employing nanotechnology approaches (such as grain boundary engineering) to regulate electron/phonon transport behavior.[57,58] Its core objective is to break the strong coupling among electrical conductivity, Seebeck coefficient, and thermal conductivity in conventional materials, ultimately achieving a significant enhancement in zT value. Furthermore, nano-modification techniques can effectively reduce the lattice thermal conductivity by tailoring the microstructure of materials (e.g., grain size, interface design, low-dimensionalization, etc.), thereby improving thermoelectric performance. This section summarizes the main strategies and recent research progress in reducing the thermal conductivity of n-type Mg_3Sb_2-based materials from the perspective of nano-modification.

2.2.1. Grain boundary engineering for grain size control

Grain boundaries (GBs) play a crucial role in thermoelectric transport, giving rise to notable differences in thermoelectric performance between single crystals and polycrystals. Due to dangling atomic bonds, local non-stoichiometry, and various defects at GBs, trap states are formed that capture charge carriers, resulting in reduced carrier mobility, electrical conductivity, and zT values. This phenomenon has been observed in numerous thermoelectric materials, including Te,[59] SiGe alloys,[60] PbTe,[61] (Hf,Zr)CoSb[62] and $Mg_3(Bi,Sb)_2$-based materials.[63] Compared with growing single crystals, preparing polycrystals with large grain sizes can potentially bring their thermoelectric performance close to that of single crystals. In recent years, methods for preparing polycrystals with large grain sizes have included prolonged high-temperature annealing,[48,52] increasing the sintering temperature,[64,65] adding extra transition metals[66] or using alloy sintering aids.[67] However, the upper limit of grain size enhancement achievable by these methods is often very limited, resulting in thermoelectric performance of polycrystals far inferior to that of single crystals. Moreover, in some of these methods, the content of volatile reactants is difficult to control at high temperatures, ultimately causing the material composition to deviate from the target. These factors lead to significantly lower zT values of polycrystalline samples compared with single crystals, especially at room and intermediate temperatures. Therefore, it is crucial to develop new strategies for preparing thermoelectric polycrystals with large grain sizes and controllable chemical compositions to achieve thermoelectric performance comparable to that of single crystals. Lei *et al.*[67] developed a method for fabricating $Mg_3(Bi,Sb)_2$-based thermoelectric polycrystals using a nano-sized sintering aid via liquid-phase sintering (Figs. 4(a)–4(c)). By adding 5 wt% nano-sized Mg_2Cu as a sintering aid to Mg_3Sb_2-based materials, the grain size was significantly increased (from 7.2 μm to 23.7 μm) through the liquid-phase sintering process. The large grains resulted in high carrier mobility (Fig. 4(d)), substantially enhancing the electrical transport performance. Meanwhile, the nanoparticles formed scattering centers at grain boundaries, reducing the room-temperature lattice thermal conductivity from 0.71 $W\cdot m^{-1}\cdot K^{-1}$ to 0.53 $W\cdot m^{-1}\cdot K^{-1}$ (Fig. 4(e)), and a zT value of 1.5 was achieved at 500 K (Fig. 4(f)).

2.2.2. Design of low-dimensional nanostructures

In recent years, low-dimensionalization has been proven to be an effective approach to improve the performance of thermoelectric materials.[25,68] The reduction in dimensionality and grain size leads to an increase in the density of states

CPB Online First Press

near the Fermi level and enhances phonon scattering, resulting in an improved Seebeck coefficient while reducing the lattice thermal conductivity. Mg_3Sb_2 is a typical layered thermoelectric material, and the anisotropy of its crystal structure leads to strong anisotropy in its thermoelectric performance. First-principles theoretical calculations have revealed that reducing dimensionality can effectively eliminate the negative impact of anisotropy and further reduce the lattice thermal conductivity. Huang *et al.*[25] employed nanotechnology to modify the structural orientation along the interlayer direction. Their results showed that two-dimensional (2D) monolayer Mg_3Sb_2 exhibits a lattice thermal conductivity approximately 60% lower than that of bulk Mg_3Sb_2 matrix materials due to quantum confinement effects and enhanced surface phonon scattering, achieving a theoretical zT value as high as 2.5 at 900 K, far exceeding the thermoelectric figure of merit of bulk materials. Compared with bulk thermoelectric materials, 2D Mg_3Sb_2-based nanothermoelectric films[69–72] are expected to become one of the most promising thermoelectric materials. Ran *et al.*[69] employed a dual-defect engineering strategy to synergistically regulate Mg vacancies and Sb-site doping with Te, achieving high-performance n-type $Mg_{3.15}Bi_{1.46}Sb_{0.5}Te_{0.04}$ thin films. The Mg-rich deposition atmosphere effectively suppressed the formation of Mg vacancies, enabling efficient n-type doping; Te doping optimized the carrier concentration and introduced lattice strain, enhancing phonon scattering and reducing the lattice thermal conductivity. The thin film achieved a high zT value of 0.47 at 525 K, the highest value reported for Mg-based thin films. Based on this film, a full $Mg_3(Sb,Bi)_2$ device (with three pairs in a π-type structure) generated an output voltage of 79 mV and a power density of 1185 $\mu W{\cdot}cm^{-2}$ under a temperature difference of 120 K. This work provides a universal design principle for thin-film thermoelectric materials and bridges the performance gap between bulk and thin-film materials in the mid-temperature range.

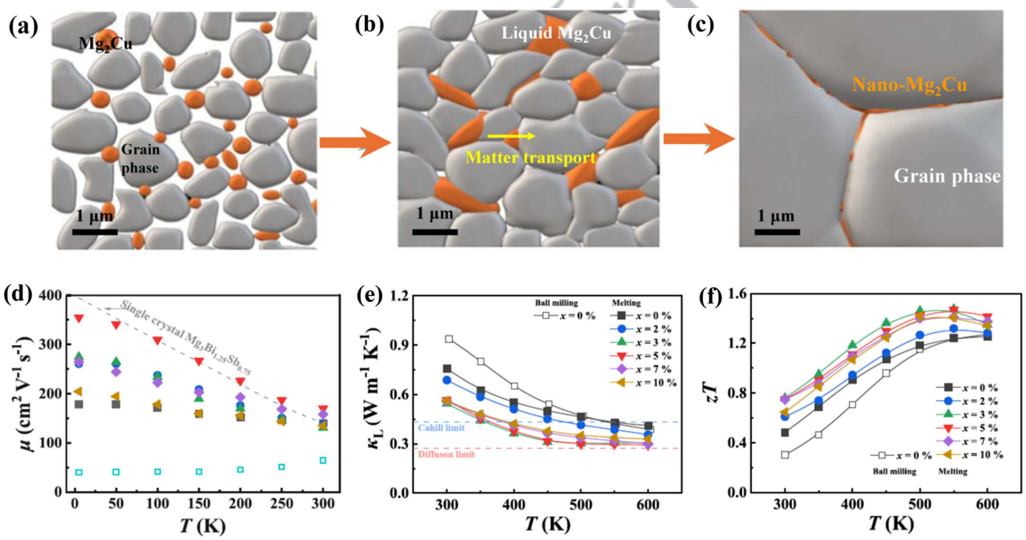


Fig. 4. A schematic diagram to fabricate large-grain materials with nano-sintering-aid by liquid-phase sintering. The three dominant stages overlap: (a) grain rearrangement, (b) solution-precipitation, and (c) Ostwald ripening; temperature dependent (d) carrier mobility, (e) lattice thermal conductivity, and (f) zT values for $Mg_{3.2}Bi_{1.195}Sb_{0.795}Te_{0.01}$-$x$ wt%Mg_2Cu ($x = 0$, 2, 3, 5, 7, 10) samples.[67]

2.3. Nanocomposite

Nanocomposite refers to a strategy that introduces a nanoscale second phase (such as nanoparticles, metallic inclusions, or low-dimensional structures) to regulate the electrical and phonon transport behavior of materials, thereby breaking the trade-off between electrical conductivity and thermal conductivity and enhancing the zT value. The core mechanism lies in utilizing the selective scattering effect of the nanophase: strongly scattering phonons to reduce the lattice thermal conductivity while minimizing the scattering of charge carriers, thus maintaining or even improving the electrical transport performance.[73] Nanomaterials exhibit physical characteristics distinctly different from those of their bulk counterparts. Incorporating nanoparticles as a second phase into thermoelectric materials to form micro/nano-structured composites is one of the approaches to improve the thermoelectric performance of Mg_3Sb_2-based materials. Recent studies have shown that nanostructures/nanocomposites[73–80] can influence local atomic arrangements through lattice strain, grain boundary reactions, or trace solid solution effects, thereby tuning the electrical and phonon transport properties. Such microstructural modifications can induce special phenomena, including a reduced Fermi level, the generation of localized resonance states, promoted convergence of valence or conduction bands, and the induction of high effective mass and interfacial energy.[81–85] In addition to improving electrical performance, this strategy also helps to hinder the propagation of thermal phonons by enhancing interfacial phonon scattering and introducing local structural disorder, thereby increasing the phonon scattering frequency. Moreover, when a co-

herent interfacial structure is formed between the nanophase and the matrix phase, the scattering of electrons can be reduced, leading to a significant improvement in the thermoelectric performance of the material. Li *et al.*[77] demonstrated that incorporating Nb/Ta nano-metallic inclusions into $Mg_3(Sb,Bi)_2$-based thermoelectric materials can significantly modulate the interfacial barrier (i.e., lower the barrier at the interface between the matrix and nano-inclusions), as shown in Fig. 5(a). The introduction of Nb/Ta nano-inclusions creates a metal–semiconductor interface with an energy barrier (E_b). This interfacial barrier can act as an energy-dependent carrier filter (low-energy electron filtering), which preferentially blocks low-energy charge carriers from crossing the interface. This filtering effect effectively increases the average carrier energy contributing to transport, thereby simultaneously maintaining or even enhancing the Seebeck coefficient while substantially improving carrier mobility and electrical conductivity, as shown in Figs. 5(b) and 5(c). This synergistic regulation of both S and σ is crucial for the significant boost in the power factor (Fig. 5(d)). As a result, a room-temperature power factor exceeding 30 $\mu W \cdot cm^{-1} \cdot K^{-2}$ was achieved. Combining the relatively wide grain size distribution of the Nb/Ta nano second phase in the composite (Fig. 5(e)) and the low lattice thermal conductivity resulting from strong phonon scattering by abundant defects (Fig. 5(f)), the $Mg_{3.1}Nb_{0.1}Sb_{1.5}Bi_{0.49}Te_{0.01}$(0.1Nb/$Mg_3Sb_{1.5}Bi_{0.49}Te_{0.01}$) composite sample exhibited more than a 200% enhancement in room-temperature zT (Fig. 5(g)). Table 2 lists the thermal transport parameters and zT values of some typical Mg_3Sb_2-based thermoelectric materials fabricated via nanocomposite approaches in recent years.[29,73,77–79]

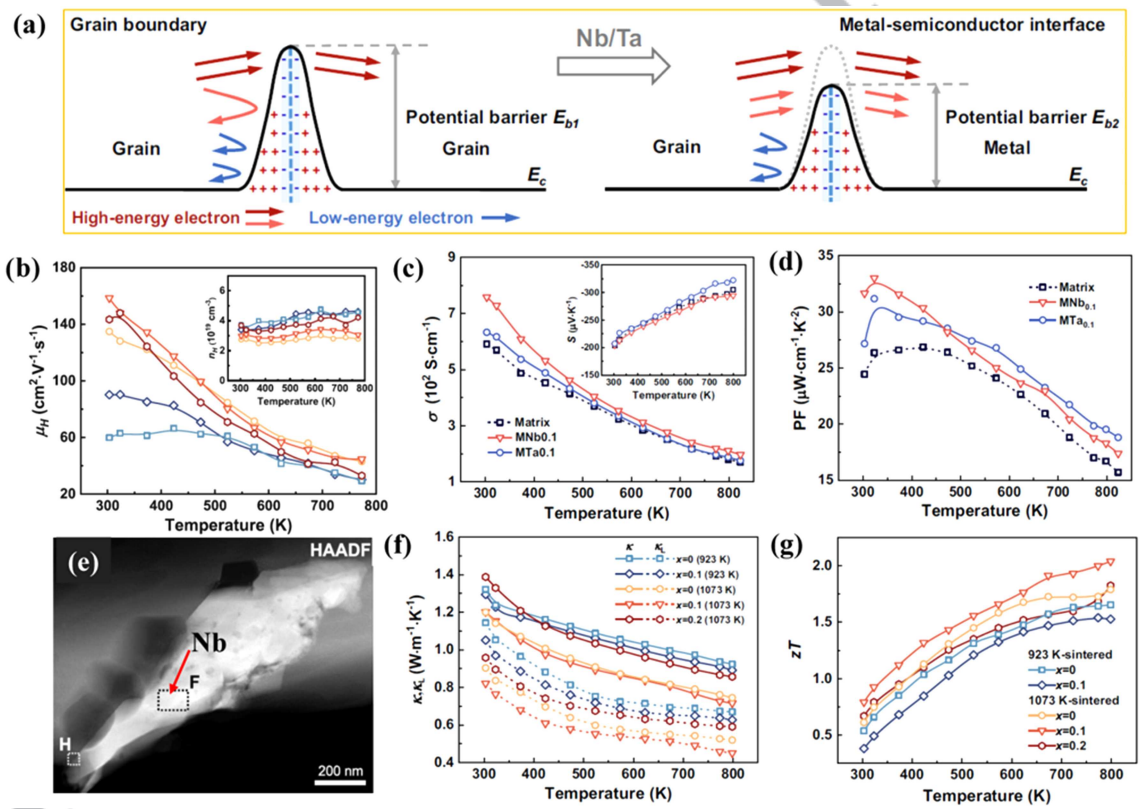


Fig. 5. (a) Schematic illustration of interfacial barriers near the grain boundary region and metal–semiconductor interface region for $Mg_{3.1}Nb_{0.1}Sb_{1.5}Bi_{0.49}Te_{0.01}$ (0.1Nb/$Mg_3Sb_{1.5}Bi_{0.49}Te_{0.01}$) sample; E_b is the interfacial potential barrier and E_c is the energy of the conduction band minimum. Temperature dependence of (c) electrical conductivity and Seebeck coefficient and (d) PF for 0.1Nb/$Mg_3Sb_{1.5}Bi_{0.49}Te_{0.01}$ and 0.1Ta/$Mg_3Sb_{1.5}Bi_{0.49}Te_{0.01}$ samples sintered at 1073 K. HAADF-STEM image of 0.1Nb/$Mg_3Sb_{1.5}Bi_{0.49}Te_{0.01}$ sample sintered at 1073 K. Temperature dependence of (b) carrier mobility, (f) total thermal conductivity and lattice thermal conductivity, and (g) zT values for xNb/$Mg_3Sb_{1.5}Bi_{0.49}Te_{0.01}$ samples sintered at 923 K and 1073 K.[77]

Table 2. Total thermal conductivity (κ), lattice thermal conductivity (κ_L), and zT values of some typical Mg_3Sb_2-based thermoelectric materials through nanocomposites.

Sample	κ ($W \cdot m^{-1} \cdot K^{-1}$)	κ_L ($W \cdot m^{-1} \cdot K^{-1}$)	zT_{max}	Ref.
$Mg_{3.3}Sb_{1.5}Bi_{0.49}Te$/0.54%$SiO_2$	0.75 @723 K	0.57 @723 K	1.31	[27]
$Mg_3Sb_{1.8}Bi_{0.2}$/GNS	0.50 @773 K	0.11 @773 K	1.35	[76]
0.1Nb/$Mg_3Sb_{1.5}Bi_{0.49}Te_{0.01}$	0.75 @1073 K	0.45 @1073 K	2.04	[77]
Mg_2Sn/Mg_3Sb_2/HCnC	0.85 @773 K	0.65 @773 K	1.13	[78]
$Mg_{3.2}SbBi_{0.99}Te_{0.01}$/MXene	0.90 @473 K	0.49 @473 K	1.40	[79]
$Mg_{3.2}SbBi_{0.99}Te_{0.01}$/0.5 wt%MWCNT	0.80 @573 K	0.45 @573 K	1.50	[80]

2.4. Synergistic regulation of electrical and thermal transport

In thermoelectric materials, synergistic regulation of electrical and thermal transport refers to integrating two or more regulation strategies (e.g., elemental doping, defect engineering, microstructural optimization, etc.) to precisely manipulate the transport behaviors of charge carriers and phonons, thereby breaking the coupling constraints among the Seebeck coefficient, electrical conductivity, and thermal conductivity, and ultimately optimizing the zT. Mg_3Sb_2-based thermoelectric materials, owing to their low cost and excellent carrier transport properties, show great potential for mid-temperature applications, but further enhancement of their thermoelectric performance is still required through the regulation of electron and phonon structures. The synergistic regulation of electrical and thermal transport mainly includes the combination of elemental doping with defect engineering, as well as the synergistic control of microstructure.

2.4.1. Elemental doping synergized with defect engineering: construction of multiscale phonon scattering centers

Elemental doping introduces point defects, dislocations, and second phases through lattice site occupancy, synergistically enhancing phonon scattering across the entire frequency spectrum and achieving efficient suppression of lattice thermal conductivity. Su *et al.*[86] demonstrated that Zn doping exhibits unique synergistic regulation advantages: on one hand, the substitution of Zn atoms at Mg sites introduces local lattice distortion, nano-sized second phases, and high-density dislocations (Figs. 6(a)–6(f)), forming multiscale phonon scattering centers, which reduce the lattice thermal conductivity of $Mg_{3.155}Zn_{0.045}Sb_{1.5}Bi_{0.49}Te_{0.01}$ to 0.54 $W{\cdot}m^{-1}{\cdot}K^{-1}$ at 773 K (Fig. 6(h)). On the other hand, this same substitution weakens ionized impurity scattering, increasing the carrier mobility to 135 $cm^2{\cdot}V^{-1}{\cdot}s^{-1}$ (Fig. 6(g)) and significantly improving the electrical performance. Combined with the low thermal conductivity, the $Mg_{3.155}Zn_{0.045}Sb_{1.5}Bi_{0.49}Te_{0.01}$ sample achieves a peak zT of 1.71 at 773 K (Fig. 6(i)). Liang *et al.*[87] adopted a synergistic approach combining lanthanide element (Dy, Tm) doping with trace sulfur (S) compensation to cooperatively regulate the electrical and thermal transport properties of Mg_3Sb_2-based materials. This combination achieves simultaneous optimization of the electronic structure and phonon transport in Mg_3Sb_2 through the collective action of multiple elements, thereby addressing the key challenge of achieving synergistic regulation of electron and phonon transport in the material. From the perspective of electronic structure, first-principles calculations show that the co-incorporation of S, Dy, and Tm shifts the Fermi level upward into the conduction band and induces multiple flat bands near the conduction band minimum, which not only promotes band convergence but also narrows the bandgap, substantially improving the n-type carrier transport efficiency. In terms of phonon transport, Dy and Tm atoms effectively hinder phonon propagation, significantly reducing the lattice thermal conductivity. The final composition $Tm_{0.03}Mg_{3.17}Sb_{1.5}Bi_{0.49}S_{0.01}$ achieves a maximum zT of 1.4 at 723 K. Finite element simulations predict that a thermoelectric module based on this composition can achieve a maximum energy conversion efficiency exceeding 9%. These findings confirm that Dy and Tm serve as efficient n-type dopants capable of simultaneously optimizing electron and phonon transport in Mg_3Sb_2, thereby significantly enhancing the thermoelectric performance of Mg_3Sb_2-based materials.

2.4.2. Microstructural synergy: combined effect of grain boundaries and dislocation networks

Constructing a cooperative structure combining coarse grains and high-density defects through process optimization can simultaneously resolve the conflict between carrier scattering at grain boundaries and phonon transport, achieving a balanced optimization of thermal conductivity and electrical performance. Lei *et al.*[67] demonstrated that the introduction of nano-sized sintering aids opens a new route for grain boundary regulation. By adding 5 wt% Mg_2Cu nanophase to $Mg_{3.2}Bi_{1.195}Sb_{0.795}Te_{0.01}$, the nano-sized sintering aid was successfully incorporated into the $Mg_3(Bi,Sb)_2$-based matrix, increasing the average grain size from 7.2 μm to 23.7 μm (Figs. 4(a)–4(c)), reducing carrier scattering at grain boundaries, and achieving a room-temperature carrier mobility of 170 $cm^2{\cdot}V^{-1}{\cdot}s^{-1}$ (Fig. 4(d)). Meanwhile, the nanoprecipitates scatter phonons, suppressing the room-temperature lattice thermal conductivity to 0.53 $W{\cdot}m^{-1}{\cdot}K^{-1}$ (Fig. 4(e)), and a zT of 1.5 is achieved at 500 K (Fig. 4(f)). Zhai *et al.*[88] achieved the synergistic construction of coarse grains and high-density dislocations in $Mg_3(Bi,Sb)_2$-based materials through Cu doping. Cu atoms form a complex segregation structure at grain boundaries, promoting grain growth to $\sim$ 10 μm. Meanwhile, a network of edge and screw dislocations along with a strong strain field forms within the grains, efficiently scattering mid-to-high frequency phonons. As a result, the $Mg_{3.2}Cu_{0.025}SbBi_{0.97}Te_{0.03}$ sample exhibits a lattice thermal conductivity as low as 0.48 $W{\cdot}m^{-1}{\cdot}K^{-1}$ at 623 K and a peak zT of 1.73. Furthermore, the Cu-doped $Mg_3(Bi,Sb)_2$-based alloy also shows excellent mechanical properties, with a plastic deformation rate of approximately 40% and a compressive stress of about 519 MPa, synergistically optimizing the electrical, thermal, and mechanical performance of $Mg_3(Bi,Sb)_2$-based alloys. The core mechanisms underlying such synergistic microstructural regulation of electrical, thermal, and mechanical performance are: (1) the coarse-grain

CPB Online In Press

structure reduces carrier scattering at grain boundaries, ensuring high electrical conductivity; (2) defects such as intragranular dislocations and nanoprecipitates form multiscale phonon scattering centers, maximizing the suppression of lattice thermal conductivity; (3) the potential mechanism for the excellent mechanical properties can be attributed to the high-density dislocation network formed within the grains, which effectively prevents the initiation and propagation of intergranular cracks, thereby ensuring high compressive strength and large plastic strain.

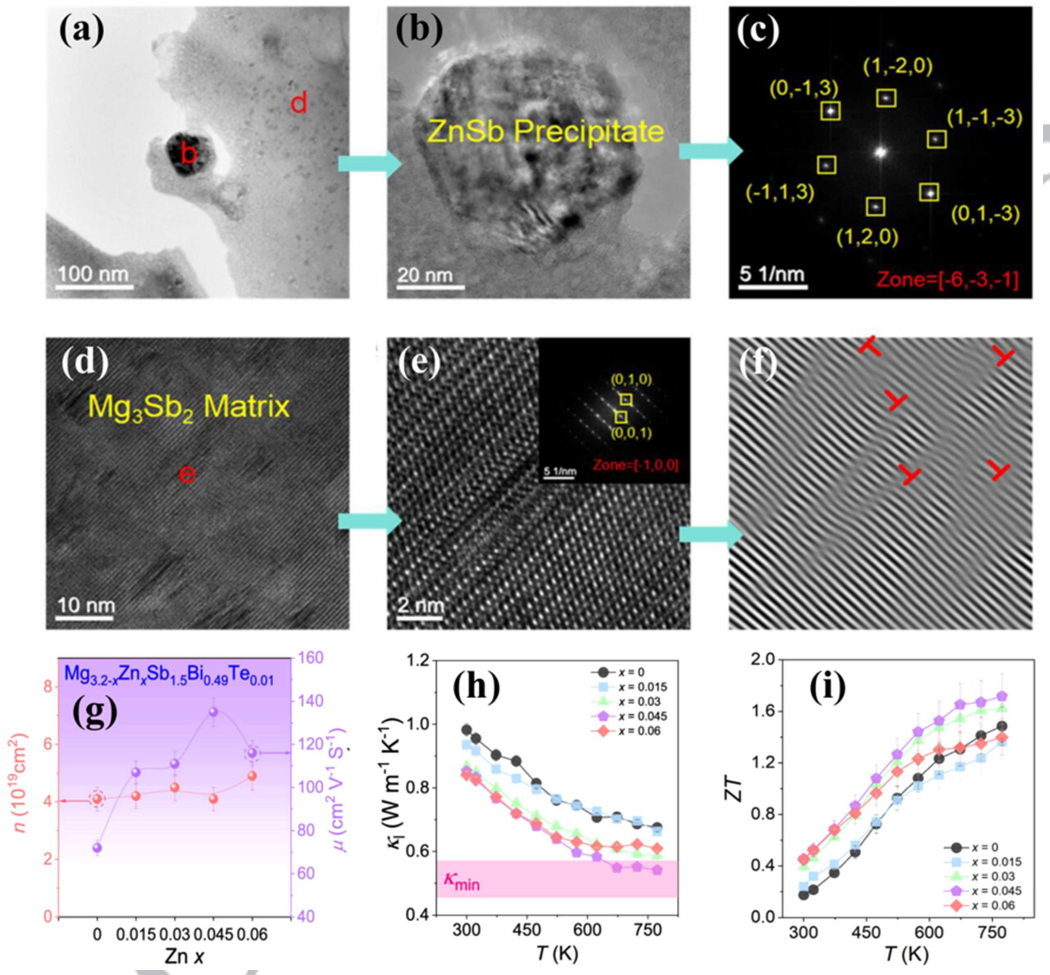


Fig. 6. (a) Transmission electron microscopy (TEM) bright-field (BF) image of $Mg_{3.155}Zn_{0.045}Sb_{1.5}Bi_{0.49}Te_{0.01}$ sample; (b) high-resolution TEM (HRTEM) image of a ZnSb precipitate; (c) selected area electron diffraction (SAED) pattern along the [−6, −3, −1] zone axis with indexed crystal information; (d) HRTEM image of the Mg_3Sb_2 matrix; (e) high-magnification HRTEM image of the matrix region shown in (d), revealing a high density of dislocations. The inset shows the SAED pattern along the [−1, 0, 0] zone axis with indexed crystal information; (f) corresponding inverse fast Fourier transform (IFFT) image, highlighting local lattice distortions caused by the dislocations; (g) Hall carrier concentration n and Hall carrier mobility μ of the $Mg_{3.2-x}Zn_xSb_{1.5}Bi_{0.49}Te_{0.01}$ ($x = 0$, 0.015, 0.03, 0.045, and 0.06) samples; temperature-dependent (h) lattice thermal conductivity κ_L and (i) ZT values of $Mg_{3.2-x}Zn_xSb_{1.5}Bi_{0.49}Te_{0.01}$ samples.[86]

3. Summary and perspectives

This review mainly summarizes the research progress in regulating the microstructure and optimizing the thermal transport properties of n-type Mg_3Sb_2-based thermoelectric materials through strategies such as alloying, doping, nanomodification, grain boundary engineering, low-dimensional nanostructure design, and nanocomposite formation. These strategies significantly enhance the phonon scattering effect through multiscale defect construction and interface optimization. The key to reducing the lattice thermal conductivity lies in achieving full-spectrum phonon scattering via the synergistic action of defects at different scales. At the atomic scale, alloying and doping effectively scatter high-frequency phonons by introducing atomic mass differences and strain field fluctuations. At the nanoscale, nanoprecipitates and low-dimensional nanostructures (e.g., nanosheets, nanowires) significantly suppress the propagation of mid-to-low frequency phonons through interfacial phonon mismatch and quantum confinement effects.

Although considerable progress has been made in n-type Mg_3Sb_2-based thermoelectric materials, several issues still warrant further investigation: (i) insufficient chemical stability hinders practical application. From the perspective of chemical stability, $Mg_3Sb_{2-x}Bi_x$ alloys react with H_2O and O_2 at room temperature, forming amorphous $Mg(OH)_2$/MgO and crystalline Bi/Sb, leading to substantial Mg loss and perfor-

mance degradation; (ii) challenges exist in material preparation processes. The sintering process has a significant impact on material performance, but the optimization of process parameters (e.g., temperature, holding time) is complex; (iii) difficulty in synergistic optimization of electrical and phonon transport. The strategies summarized above for optimizing thermal transport properties can effectively reduce thermal conductivity, but they also strongly scatter charge carriers, leading to deteriorated electrical performance. Therefore, better strategies are still needed for synergistic electrical–phonon transport optimization; (iv) while optimizing the thermoelectric performance of n-type Mg_3Sb_2-based materials, considering practical applications, the enhancement of their mechanical properties is also crucial for the development of thermoelectric devices.

In summary, the regulation of thermal transport properties in n-type Mg_3Sb_2-based thermoelectric materials has evolved from single-defect design toward a new stage featuring multi-scale and multi-mechanism synergistic optimization. Through the integrated combination of cross-scale structural engineering, advanced fabrication techniques, and theoretical simulations, it is expected to overcome the performance bottleneck of achieving a zT value exceeding 3.0, thereby laying a solid foundation for the practical application of next-generation low-to-medium temperature thermoelectric materials.

Acknowledgements

This review was supported by the State Key Laboratory of Advanced Technology for Materials Synthesis and Processing (Wuhan University of Technology) (Grant No. 2025-KF-5) and Excellent Youth Project of Natural Science Foundation of Anhui Province of China (Grant No. 2208085Y17).

References

[1] Disalvo F J 1999 *Science* **285** 703
[2] Snyder G J and Toberer E S 2008 *Nat. Mater.* **7** 105
[3] Li X J, He W K and Zhao L D 2025 *Mater. Lab* **4** 240010
[4] Lu W B, Luo W, Fan Y C, Ding Q and Jiang G 2024 *Adv. Ceram.* **45** 177 (in Chinese)
[5] Huang K, Wang Z Y, Wang C Y, Zhang Y X, Jiang Y H, Feng J and Ge Z H 2026 *J. Adv. Ceram.* **15** 9221239
[6] Liu Z Y, Zhu J L, Tong X, Niu S and Zhao W Y 2020 *J. Adv. Ceram.* **9** 647
[7] Yang L, Chen Z G, Dargusch M S and Zou J 2018 *Adv. Energy Mater.* **8** 1701797
[8] Zhao W Y, Liu Z, Sun Z G, Zhang Q J, Wei P, Mu X, Zhou H Y, Li C C, Ma S F, He D Q, Ji P X, Zhu W T, Nie X L, Su X L, Tang X F, Shen B G, Dong X L, Yang J H, Liu Y and Shi J 2017 *Nature* **549** 247
[9] Liu Z Y, Yang T, Wang Y G, Ruan X F, Jin C G and Xia A L 2023 *J. Eur. Ceram. Soc.* **43** 1985
[10] Basu R and Singh A 2021 *Mater. Today Phys.* **21** 100468
[11] Wei T R, Qiu P, Zhao K, Shi X and Chen L 2023 *Adv. Mater.* **35** 2110236
[12] Prunet G, Pawula F, Fleury G, Cloutet E, Robinson A J, Hadziioannou G and Pakdel A 2021 *Mater. Today Phys.* **18** 100402
[13] Wang Q, Zhou Z F, Liu C, Zheng Y P, Shi Z M, Wei B, Zhang W Y, Nan C W and Lin Y H 2026 *Chem. Soc. Rev.* **55** 358
[14] Cao T, Shi X L, Li M, Hu B, Chen W, Liu W D, Lyu W, Macleod J and Chen Z G 2023 *eScience* **3** 36
[15] Liu Z Y, Ma J J, Zeng Z P, Ma N, Ba Q, Zhang D, Tao Z and Xia A L 2026 *Acta Phys. Sin.* **75** 030815 (in Chinese)
[16] Wu H, Shi X L, Duan J, Liu Q and Chen Z G 2023 *Energy Environ. Sci.* **16** 1870
[17] Biswas K, He J Q, Blum I D, Wu C I, Hogan T P, Seidman D N, Dravid V P and Kanatzidis M G 2012 *Nature* **489** 414
[18] Liu D R, Wang, D Y, Hong T, Wang Z Y, Wang Y P, Qin Y X, Su L Z, Yang T Y, Gao X, Ge Z H, Qin B C and Zhao L D 2023 *Science* **380** 841
[19] Shi X L, Tao X Y, Zou J and Chen Z G 2020 *Adv. Sci.* **7** 1902923
[20] Moshwan R, Yang L, Zou J and Chen Z G 2017 *Adv. Funct. Mater.* **27** 1703278
[21] Tan G J, Shi F Y, Doak J W, Sun H, Zhao L D, Wang P L, Uher C, Wolverton C, Dravid V P and Kanatzidis M G 2015 *Energy Environ. Sci.* **8** 267
[22] Hong M, Li M, Wang Y, Shi X L and Chen Z G 2023 *Adv. Mater.* **35** 2208272
[23] Tamaki H, Sato H K and Kanno T 2016 *Adv. Mater.* **28** 10182
[24] Toberer E S, May A F and Snyder G J 2010 *Chem. Mater.* **22** 624
[25] Huang S, Wang Z, Xiong R, Yu H and Shi J 2019 *Nano Energy* **62** 212
[26] Liang J, Yang H, Liu C, Miao L, Chen J, Zhu S, Xie Z, Xu W, Wang, X, Wang J, Peng B and Koumoto K 2020 *ACS Appl. Mater. Interfaces* **12** 21799
[27] Gao J L, Zhao H L and Xu Y L 2023 *Acta Phys. Sin.* **72** 117102 (in Chinese)
[28] Shang H, Liang Z, Xu C, Mao J, Gu H, Ding F and Ren Z 2020 *Research* **2020** 1219461
[29] Iqbal Y, Wang C, Hussain S, Wang J, Abohashrh M, Ahmad I, Shahzad A, Adil M, Ullah S, Li L and Li S 2025 *J. Mater. Eng. Perform* **35** 2466
[30] Ran Y, Ma W, Yu H, Li W, Zhou D, Wang F, Gao N, Yu Z and Tai K 2024 *J. Alloys Compd.* **985** 174028
[31] He S, Ma Y, Li X, Zhong H, Luo X, Xia Z, Zhang Y, Yan K, Liang Z and Xie H 2024 *J. Alloys Compd.* **1005** 176003
[32] Luo H R, Shi X L, Liu Y Q, Li M, Zhang M, Luo X H, Wang M R, Huang X P, Hu L P and Chen Z G 2025 *Nat. Commun.* **16** 3136
[33] Alam H and Ramakrishna S 2013 *Nano Energy* **2** 190
[34] Peng W, Petretto G, Rignanese G M, Hautier G and Zevalkink A 2018 *Joule* **2** 1879
[35] Zhang Z, Li J, Yao H, Wang Q, Yin L, Liu K, Ma X, Yuan M, Wang R, Duan S, Bao X, Cheng J, Wang X, Li X, Shuai J, Sui J, Lin X, Tan X, Liu X, Mao J, Xie G and Zhang Q 2024 *Acta Mater.* **268** 119777
[36] Chen Y, Li L, Li S, Yang G, Peng P and Wang C 2022 *J. Phys. D: Appl. Phys.* **55** 434001
[37] Imasato K, Kang S D, Ohno S and Snyder G J 2018 *Mater. Horiz.* **5** 59
[38] Li G, Bajaj S, Aydemir U, Hao S, Xiao H, Goddard W A, Zhai P, Zhang Q and Snyder G J 2016 *Chem. Mater.* **28** 2172
[39] Quarez E, Hsu K F, Pcionek R, Frangis N, Polychroniadis E and Kanatzidis M G 2005 *J. Am. Chem. Soc.* **127** 9177
[40] Lee M H, Byeon D G, Rhyee J S and Ryu B 2017 *J. Mater. Chem. A* **5** 2235
[41] Zhao C, Li Z, Fan T, Xiao C and Xie Y 2020 *Research* **2020** 9652749
[42] Wood M, Imasato K, Anand S, Yang J and Snyder G J 2020 *J. Mater. Chem. A.* **8** 2033
[43] Zhang J W, Song L R, Mamakhel A, Jørgensen M R V and Iversen B B 2017 *Chem. Mater.* **29** 5371
[44] Mo X, Liao J, Yuan G, Zhu S, Lei X, Huang L, Zhang Q, Wang C and Ren Z 2022 *J. Magnes. Alloys* **10** 1024
[45] Mao J, Wu Y, Song S, Shuai J, Liu Z, Pei Y and Ren Z 2017 *Mater. Today Phys.* **3** 1
[46] Gorai P, Toberer E S and Stevanović V 2019 *J. Appl. Phys.* **125** 25105
[47] Chen, X X, Zhu J B, Qin D D, Qu N, Xue W H, Wang Y M, Zhang Q, Cai W, Guo F K and Sui J H 2021 *Sci. China Mater.* **64** 1761
[48] Shi X, Zhao T, Zhang X, Sun C, Chen Z, Lin S, Li W, Gu H and Pei Y 2019 *Adv. Mater.* **31** 1970253
[49] Mao J, Shuai J, Song S, Wu Y, Dally R, Zhou J, Liu Z, Sun J, Zhang Q, Dela Cruz C, Wilson S, Pei Y, Singh D J, Chen G, Chu C W and Ren Z 2017 *Proc. Natl. Acad. Sci. USA* **114** 10548
[50] Jiang Y, Ferhat M, Fan W H, Chen S P, Wang Y C, Chen J, Al-Yusufi, R A A and Dun C C 2022 *Chem. Eng. J.* **446** 136981
[51] Zhang J W, Song L R and Iversen B B 2020 *Adv. Sci.* **7** 2002867

CPB Online First Press

[52] Lei J, Wuliji H, Zhao K, Wei T R, Xu Q, Li P, Qiu P and Shi X 2021 *J. Mater. Chem. A* **9** 25944

[53] Zhang J W, Song L R and Iversen B B 2021 *ACS Appl. Mater. Interfaces* **13** 10964

[54] Chen X, Wu H, Cui J, Xiao Y, Zhang Y, He J, Chen Y, Cao J, Cai W, Pennycook S J, Liu Z, Zhao L D and Sui J H 2018 *Nano Energy* **52** 246

[55] Yu L, Shi X L, Mao Y, Liu W D, Ji Z, Wei S, Zhang Z, Song W, Zheng S and Chen Z G 2024 *ACS Nano* **18** 1678

[56] Li J W, Liu W, Xu W, Zhuang H L, Han Z, Jiang F, Zhang P, Hu H, Gao H, Jiang Y, Cai B, Pei J, Su B, Li Q, Hayashi K, Li H, Miyazaki Y, Cao X, Zheng Q and Li J F 2023 *Adv. Mater.* **35** 2209119

[57] Chen W, Shi X L, Li M, Liu T, Mao Y, Liu Q, Dargusch M, Zou J, Lu G Q and Chen Z G 2024 *Science* **386** 1265

[58] Ibn Shamsah M S 2024 *Energies* **17** 5002

[59] Wu Y, Liu F, Zhang Q, Zhu T, Xia K and Zhao X 2020 *J. Mater. Chem. A.* **8** 8455

[60] Yonenaga I, Li W, Akashi T, Ayuzawa T and Goto T 2005 *J. Appl. Phys.* **98** 063702

[61] Kishimoto K, Tsukamoto M and Koyanagi T 2002 *J. Appl. Phys.* **92** 5331

[62] Qiu Q, Liu Y, Xia K, Fang T, Yu J, Zhao X and Zhu T 2019 *Adv. Energy Mater.* **9** 1803447

[63] Kuo J J, Kang S D, Imasato K, Tamaki H, Ohno S, Kanno T and Snyder G J 2018 *Energy Environ. Sci.* **11** 429

[64] Han Z, Gui Z, Zhu Y B, Qin P, Zhang B P, Zhang W, Huang L and Liu W 2020 *Research* **2020** 1672051

[65] Luo T, Kuo J J, Griffith K J, Imasato K, Cojocaru-Mirédin O, Wuttig M, Gault B, Yu Y and Snyder G J 2021 *Adv. Funct. Mater.* **31** 2100258

[66] Wang L, Sato N, Peng Y, Chetty R, Kawamoto N, Nguyen D H and Mori T 2023 *Adv. Energy Mater.* **13** 2370143

[67] Lei J, Zhao K, Liao J, Yang S, Zhang Z, Wei T R, Qiu P, Zhu M, Chen L and Shi X 2024 *Nat. Commun.* **15** 6588

[68] Hicks L D and Dresselhaus M S 1993 *Phys. Rev. B* **47** 16631

[69] Ran Y J, Ma W X, Li W X, Li S Q, Wang X Y, Xiong T, Zhou D Y, Kong X S, Gao N, Yu Z and Tai K P 2026 *Acta Mater.* **308** 122012

[70] Ran Y J, Ma W X, Yu H L, Li W X, Zhou D Y, Wang F, Gao N, Yu Z and Tai K P 2024 *J. Alloys Compd.* **985** 174028

[71] Xie S, Liu W, Wan X L, Lyu J A, Yan F, Ouyang Y J, Li X D, Liu Y, Wang Z Y, Wang R, Wu J S, Zhang Q J and Tang X F 2023 *Adv. Funct. Mater.* **33** 2300154

[72] Hu B, Shi X L, Cao T, Zhang M, Chen W, Liu S, Li M, Liu W and Chen Z G 2025 *Adv. Sci.* **12** 2502683

[73] Bhardwaj A, Misra D K, Pulikkotil J J, Auluck S, Dhar A and Budhani R C 2012 *Appl. Phys. Lett.* **101** 133103

[74] Misra D, Bhardwaj A and Singh S 2014 *J. Mater. Chem. A* **2** 11913

[75] Nielsch K, Bachmann J, Kimling J and Böttner H 2011 *Adv. Energy Mater.* **1** 713

[76] Bhardwaj A, Shukla A K, Dhakate S R and Misra D K 2015 *RSC Adv.* **5** 11058

[77] Li J W, Han Z, Yu J, Zhuang H L, Hu H, Su B, Li H, Jiang Y, Chen L, Liu W, Zheng Q and Li J F 2023 *Nat. Commun.* **14** 7428

[78] Zhu Y, Han Z, Han B, Jiang F, Wu X, Han C G, Deng Y and Liu W 2021 *ACS Appl. Mater. Interfaces* **13** 56164

[79] Sauerschnig P, Naruke M, Imasato K, Yamamoto A, Ishida T and Ohta M 2025 *Chem. Mater.* **37** 7240

[80] Liang Z X, Xu C C, Shang H J, Ning M H, Tong T, Song S W, Ren W Y, Shi X, Liu X, Ding F Z, Bao J M, Wang D Z and Ren Z F 2023 *Adv. Energy Mater.* **13** 2301107

[81] Heremans J P, Jovovic V, Toberer E S, Saramat A, Kurosaki K, Charoenphakdee A, Yamanaka S, Snyder G J 2008 *Science* **321** 554

[82] Wang S, Tan X, Tan G, She X, Liu W, Li H, Liu H and Tang X 2012 *J. Mater. Chem.* **22** 13977

[83] Pei Y, Shi X, Lalonde A, Wang H, Chen L and Snyder G J 2011 *Nature* **473** 66

[84] Liu W, Tan X, Yin K, Liu H, Tang X, Shi J, Zhang Q and Uher C 2012 *Phys. Rev. Lett.* **108** 166601

[85] Kosonowski A, Kumar A, Parashchuk T, Cardoso-Gil R and Wojciechowski T K 2021 *Dalton Trans.* **50** 1261

[86] Su H, Shi W, Zhang Y, Lin Y and Liu Y 2025 *ACS Appl. Energy Mater* **8** 3942

[87] Liang J X, Yu L, Luo S T, Dong L X, Wei Z B, Wang T, Jiang Y T, Zheng S Q, Song W Y and Wang H C 2025 *ACS Appl. Energy Mater.* **8** 12760

[88] Zhai L, Liu H, Shi J, Cheng L, Gao L, Yang Z, Zhang X, Liu L, Su L, Zhang Y, Fan W, Xie W and Sun Z 2026 *Acta Mater.* **303** 121719

CPB Online IP Press